Research Article

Manar. Lo. Dayekh*, Amin Ghadi and Saleem A. Hussain

Preparation and investigation of cobalt nanoparticles by laser ablation: Structure, linear, and nonlinear optical properties

https://doi.org/10.1515/eng-2024-0002 received January 04, 2024; accepted February 28, 2024

Abstract: In this study, cobalt nanoparticles (CoNPs) were prepared by using an Nd-YAG pulsed laser at a wavelength of 1,064 nm and an energy of 800 mJ. From the results of the structural and morphological attributes of CoNP films, it is evident that CoNPs exhibit different spherical configurations with diameters spanning from a few nanometers to 24 nm. The surfaces of these CoNP films indicate that they exhibit a certain degree of homogeneity and uniform vertical heights. Additionally, the results demonstrate an increase in granular size growth and the emptying of cavities on the material's surface. The absorption curves appeared as a function of the wavelength within the range of 300-1,000 nm and the peak absorption of CoNPs in the ultraviolet radiation region, and the prohibited energy gap for direct transitions was known, and the value is 4 eV, while the nonlinear optical properties showed that the particles show a nonlinear refractive index (self-defocusing) and a nonlinear absorption cobalt coefficient with the absorption of two photons; thus, the CoNPs possess good nonlinear properties and can be used in nonlinear optical photonic device, optical power limiter, and a wide range of nonlinear applications.

Keywords: CoNPs, laser ablation, structure, optical properties

1 Introduction

The field of nanotechnology, which is seeing significant growth, encompasses the development and fabrication of

Saleem A. Hussain: Department of Physics of Education, Al-Qadisiyah University, Qadisiyah, Iraq

diverse nanomaterials. Nanoparticles (NPs) are defined as objects ranging in size from 1 to 100 nm, which exhibit distinct properties compared to their bulk counterparts as a result of their reduced dimensions. Currently, a range of metallic nanomaterials is being synthesized using copper, zinc, titanium, magnesium, gold, alginate, silver, and cobalt. NPs find extensive utilization throughout several domains, including medical interventions, energy storage in solar and oxide fuel batteries, as well as widespread integration into numerous everyday commodities such as clothes and cosmetics [1,2]. The increasing need for nanomaterials, coupled with the realization that achieving high efficiency is not the sole objective in numerous industrial and technological applications, has prompted the development of diverse production methods for these materials. This diversification holds significant promise in terms of both quantitative and qualitative advancements, particularly in the medical domain, which has historically been challenging to access due to its high economic costs [1,3]. The techniques or procedures discussed herein are characterized by their operation at the atomic level in order to attain desired outcomes. Furthermore, it is observed that alterations in the mass scale of a given substance lead to corresponding differences in its chemical reactivity. Based on the observed increase in chemical activity, it may be inferred that as the scale decreases, the chemical activity proportionally increases. The acceleration of preparedness for nanoscience and nanotechnology is being driven by global technical advancements in several sectors. There are two fundamental sorts of technologies, namely top-down and bottom-up technologies [4]. NPs employ a top-down approach to selectively remove material and create smaller structures from bigger ones through etching. In contrast, a material is constructed by a bottomup approach, wherein it is systematically assembled atom by atom, molecule by molecule, or cluster by cluster [3]. The creation of NPs using pulsed laser ablation (PLA) of solid samples submerged in liquid has been shown to possess considerable potential [4]. The earliest description of the development of PLA at the solid-liquid interface for the purpose of creating iron oxides with metastable phases

^{*} Corresponding author: Manar. Lo. Dayekh, Faculty of Basic Science, University of Mazandaran, Babolsar, Iran, e-mail: manar physics@yahoo.com Amin Ghadi: Faculty of Basic Science, University of Mazandaran, Babolsar, Iran

was provided by Patil et al. in 1987. The aforementioned procedure was conducted by subjecting a pure iron target to ablation in a water medium, employing a pulsed laser. The technique referred to as liquid phase pulsed laser ablation (LP-PLA) is denoted by this nomenclature [5]. The utilization of PLA in liquids is a novel approach to the synthesis of NPs in a colloidal solution [6]. The process is uncomplicated and does not necessitate any knowledge of chemistry. Moreover, it is not limited in its scope as it can generate NPs without the need for counter ions or surface-active molecules [7]. Cobalt is considered one of the important materials in technological, industrial, and medical applications, and it has various uses due to its properties, including ferromagnetism, hardness, and corrosion resistance, in addition to the high melting degree and multiple equalities [8]. The particles of nano-cobalt are promising with exceptional motivational material for the magnetic, chemical, and electronic properties. Since the nanoscale and the developed surface open wide field in the application of cobalt nanoparticles (CoNPs) in optical methods and biomedicine in addition to other fields and the application of particles in many therapeutic and diagnostic agents and magnetic resonance imaging [9]. Cobalt has garnered significant attention owing to its distinctive characteristics and a wide range of applications. Nevertheless, it is important to acknowledge that the exceptional characteristics of cobalt have garnered more fascination due to the revelation of atypical physical and chemical attributes exhibited by CoNPs [2]. In this study, CoNPs were prepared by the pulsed Nd-YAG laser deposition method, and structure, linear, and nonlinear optical properties were studied. The results obtained are good and interesting and can be developed and used to be certified for the manufacture of optical sensors, optical solar cells, and other optical devices. The results also showed high nonlinear optical effects, which qualify them as good and promising materials for applications in nonlinear optical photonic devices, optical power selectors, and a wide range of nonlinear optical applications.

Various methods are employed to measure the nonlinear optical properties of the material. The Z-scan approach is the most straightforward method for evaluating the attributes associated with its exceptional sensitivity to a solitary laser beam [10]. The Z-scan technique was employed to measure the magnitude and sign of nonlinear features [11]. This technique has been employed to ascertain the nonlinear optical properties of several substances, including liquid crystals, organic or carbon-based molecules, dielectrics, and semiconductors [12]. The essential geometry is shown in Figure 1.

The Z-scan technique is based on the assumption that the sample is moved down the Z-axis, passing past the focal point of the Gaussian beam. The interaction between the laser light and the medium varies as the sample moves. The variation in intensities of the sample is attributed to its positional relationship (z) with respect to the focal point (z = 0) [11]. In the conventional procedure, it is customary to position the specimen precisely at the focal point of the lens and thereafter displace it incrementally along the z-axis at a distance denoted as z_0 , where z represents the Rayleigh length [14]

$$z_0 = \frac{\omega_0^2}{\lambda} \pi, \tag{1}$$

where ω_0 is the radius of the laser beam and λ represents the wavelength.

The ways to use Z-scan: Close aperture and Open aperture. When measuring nonlinear absorption, the open aperture Z-scan is utilized, whereas when measuring nonlinear refraction, the tight aperture Z-scan is followed [14].

The change in temperature, denoted as ΔT , exhibits a direct relationship with the nonlinear phase shift, $\Delta \Phi_{\rm o}$, as stated in Kumari et al. [14]. It is commonly observed that the disparity between the maximum and minimum magnitudes of the normalized transmittance serves as a reliable diagnostic of nonlinearity

$$\Delta T_{\rm p-v} = 0.406 |\Delta \Phi_{\rm o}|, \tag{2}$$

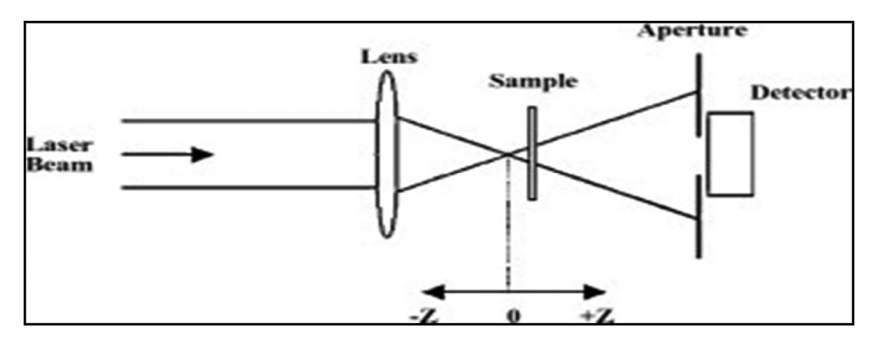


Figure 1: Z-scan experimental arrangement [13].

where 0.406 is the constant quantity. And

$$\Delta\Phi_0 = k n_2 I_0 L_{\text{eff}},\tag{3}$$

where $\Delta\Phi_0$ is the nonlinear phase shift, k represents the wave number [15], and I represents the initial laser beam intensity at focus z = 0.

$$I_0 = P/2\pi w_0^2$$
. (4)

While the laser beam's radius is wo and its power is P.In addition,

$$L_{\text{eff}} = (1 - \exp^{(-\alpha t)}/\alpha), \tag{5}$$

where $L_{\rm eff}$ is the sample's effective thickness [16].

The nonlinear refraction index, denoted as n_2 , is demonstrated via

$$n_2 = \Delta \Phi / k I_0 L_{\text{eff}}. \tag{6}$$

The relationship between the change in the nonlinear refractive index (Δn) and the intensity of a laser beam (I_0) can be expressed as follows:

$$\Delta n = n_2 I_0. \tag{7}$$

The nonlinear absorption coefficient can be counted from the open aperture curve utilizing the following formula [17]:

$$\beta = \frac{2\sqrt{2}}{I_0 L_{\text{eff}}} \Delta T,\tag{8}$$

where the variable ΔT represents the occurrence of a singular peak or singular valley on the Z-scan curve when an open aperture is utilized. The third-order nonlinear optical susceptibility $\chi^{(3)}$ can be understood in terms of two relationships (9) and (10). These connections establish that the real component of $\chi^{(3)}$ corresponds to the nonlinear refraction index, while the virtual component corresponds to the nonlinear absorption coefficient [18]

$$\text{Re}[\chi^{(3)}](\text{esu}) = 10^{-4} \frac{\epsilon_0 c^2 n_0^2 n_2}{\pi} \left(\frac{\text{cm}^2}{\text{W}}\right),$$
 (9)

Im[
$$\chi^{(3)}$$
](esu) = $10^{-2} \frac{\epsilon_0 c^2 n_0^2 \lambda \beta}{4\pi^2} \left[\frac{\text{cm}^2}{\text{W}} \right]$. (10)

The following equation (11) can be employed to represent the magnitude of the third-order nonlinear optical susceptibility, denoted as $|\chi^{(3)}|$

$$|\chi^{(3)}| = [\text{Re}(\chi^{(3)}) + \text{Im}(\chi^{(3)})]^{1/2}.$$
 (11)

2 Experimental method

PLA was used to prepare CoNPs from cobalt metal fragments that had been purified using ethanol solution and distilled water to remove impurities. The Nd-YAG pulse laser system with a wavelength of 1,064 nm, a capacity of 800 mJ, a pulse count of 1,500 pulses, a repetition rate of 6 Hz, and a beam diameter of 2 mm in the water solution was utilized to prepare the CoNPs. In order to produce CoNPs, a laser beam with a wavelength of 1,064 nm was pointed onto a cobalt metal target submerged in 3 ml of distilled water in Baker. After that CoNPs were deposited and dried on glass bases, the structure properties were studied using the FE-SEM study (TESCAN Mira3-, Czech Republic), and the atomic force microscope (AFM; NT-MDT, NTEGRA AFM, Ireland) was used with the specifications. The optical features of films formed of CoNPs have been studied at wavelengths between 300 and 1,100 nm using a Mega-2100 Dual UV-Vis Spectrophotometer. The nonlinear optical characteristics of CoNP films are described using Z-scan techniques to determine the nonlinear optical properties.

3 Results and discussion

3.1 Result of microscopy via field emission scanning electron (FESEM) tests

FESEM screening images of CoNPs prepared by a 1,064 nm Nd-YAG pulsed laser deposited on a glass substrate were obtained to determine their shape. The morphological images of the cobalt particle surfaces that have been eliminated in distilled water exhibit increased granular size, spherical shape, and homogeneous with distinctive shapes. Images taken at a magnification of 200k× allow us to observe that the surfaces of cobalt particles are free of islands, have a homogeneous distribution, and clearly demonstrate an increase in the rate of granular size. Thus, we notice through images at the shape (200 nm, 1 µm) that cobalt particles are composed of nano-structured granules and arranged regularly. These grains with spherical structures showed distinctive shapes, and the diameter of the NPs ranging from a few nanometers to 24 nm was calculated as seen in Figure 2.

3.2 Surface texture analysis (AFM)

Figure 3 displays the atomic force microscopy pictures of CoNPs that were synthesized using pulsed Nd-YAG laser ablation in water, having a wavelength of 1,064 nm. These NPs were then deposited on glass substrates. The dimensions of the captured image were $2 \mu m \times 2 \mu m$. The findings indicate that the membrane materials exhibit a certain degree of homogeneity and uniform vertical heights, as observed in both two- and three-dimensional testing. Additionally, the results demonstrate

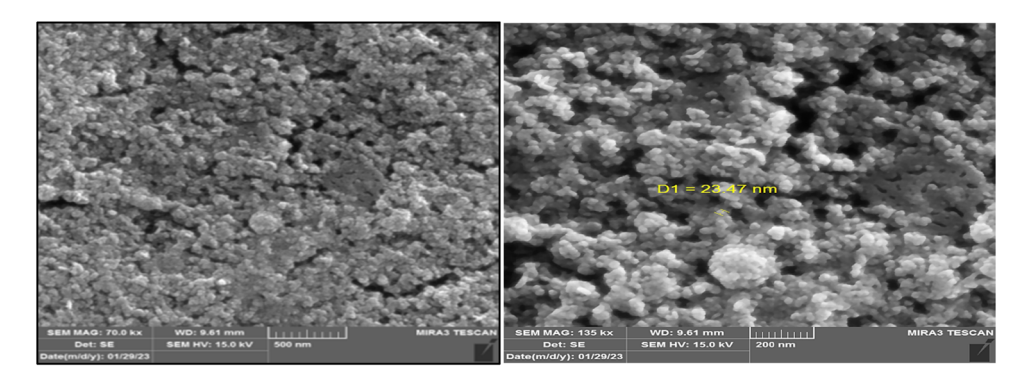


Figure 2: FESEM examination images of CoNPs deposited on glass substrates.

an increase in granular size growth and the absence of cavities on the material's surface. Table 1 illustrates the morphological characteristics of the CoNP films that were created.

3.3 Optical measurements

3.3.1 Linear optical properties

The optical properties of any material are the properties that must be known in order to know the nature of the material and its uses in different applications, and information can be obtained on the optical properties by measuring the absorption and permeability spectrum of different wavelengths and through which the optical constants are calculated, and the optical energy gap is known. Here are some of the results that are calculated for CoNPs.

Table 1: Topographical characteristics of CoNPs prepared by pulsed Nd–YAG laser ablation having a wavelength of 1,064 nm

Sample	Root mean square Sq (nm)	Roughness average Sa (nm)	
CoNPs (1064)	20.0167	15.3807	

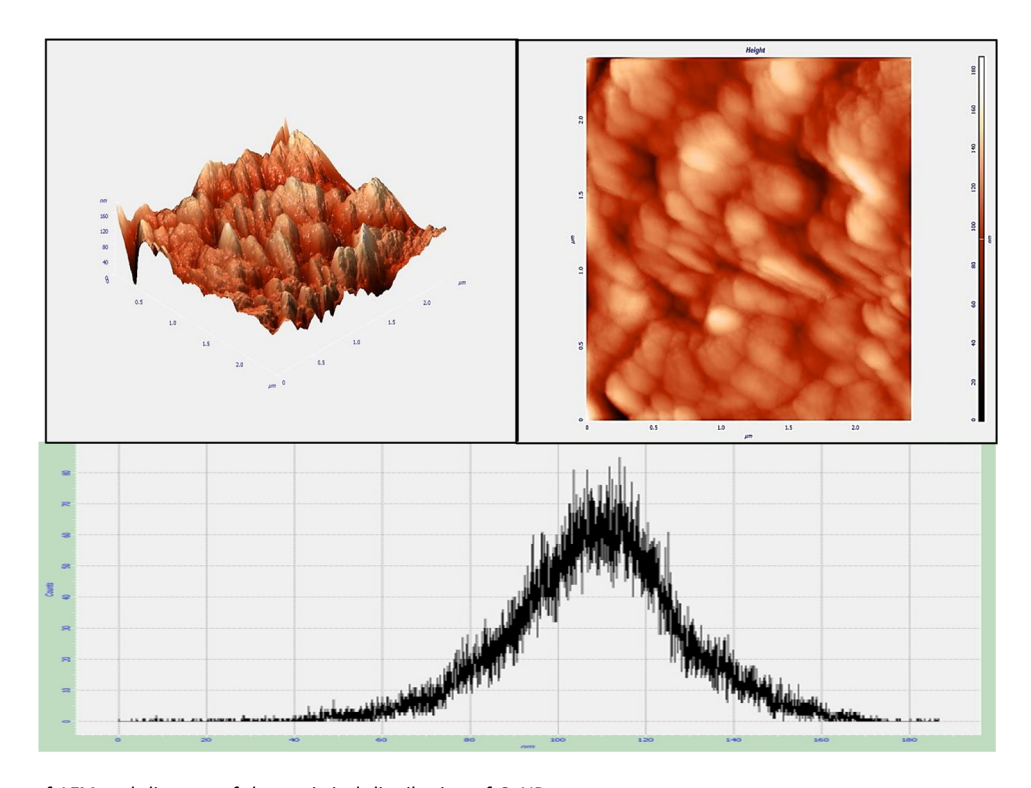


Figure 3: Images of AFM and diagram of the statistical distribution of CoNPs.

Figure 4 shows the change in the absorption spectrum of the aqueous solution of CoNPs suspended in water as a function of the wavelength (300–1,100 nm) and the appearance of CoNP peaks at 400 and 700 nm. The reason for the existence of these peaks is due to the average size of the NPs produced with the laser pulse used in the scraping process, due to the formation of NPs and thus increased absorption. Also, the surface plasmon resonance distribution of CoNPs depends on the methods of preparation of NPs, which indicates different particle distribution and morphology of NPs as indicated by previous research [19–21].

The transmittance spectra of CoNP films, which had a thickness of 200 nm, were analyzed within the wavelength range of 300-1,100 nm. The quantity of energy levels, which is associated with the chemical composition and crystalline properties of matter, constitutes one of the factors influencing transmittance spectra. Moreover, the thickness of a material plays a pivotal role in the process of matter transfer. Figure 5 displays the transmittance spectra of films composed of CoNPs, illustrating the relationship between transmittance and wavelengths. The transmission and absorbance spectra exhibit inverse behavior. The data illustrate the relationship between transmittance and wavelength, indicating a decrease in transmittance as the wavelength decreases and an increase in transmittance as the wavelength increases. According to the data presented in Figure 5, it can be observed that the transmittance attains its maximum value of 75.84% at wavelengths equal to and greater than 1,098.

Figure 6 illustrates the connection between the absorbance coefficient (α), which depends on the energy of the incident photon (hv). When the absorbance coefficient exceeds (10^4 cm⁻¹), transfers are regarded as direct transfers. The absorption coefficient (α) of CoNPs with a thickness of

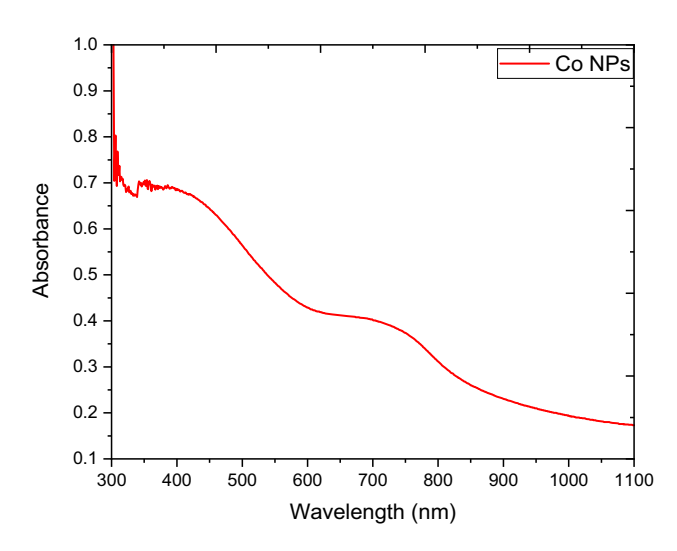


Figure 4: Absorbance versus wavelength for CoNPs.

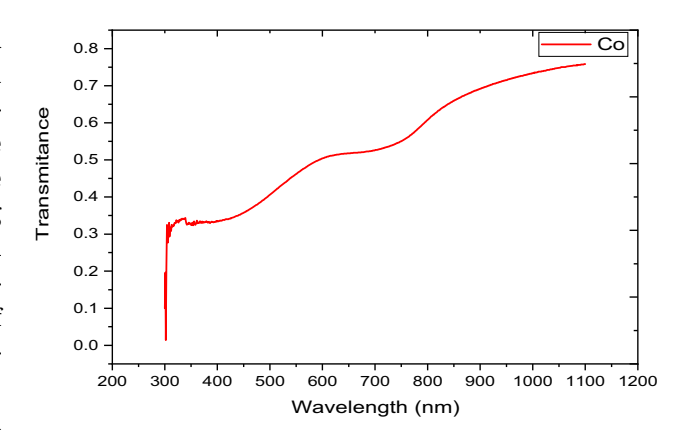


Figure 5: Transmittance versus wavelength for CoNPs.

200 nm was determined [10] using relation (12). The absorption coefficient (α) is dependent on the energy of the incident photons as well as on the characteristics of the material, which include energy gaps and different types of electronic transmission that occur between frequency bands.

$$\alpha = 2.303A/t,\tag{12}$$

where α is the absorption coefficient, A is the absorbance, and t is the thickness of film.

The reflection coefficient of CoNPs deposited on glass was determined using the following relationship (13):

$$n_0 = \frac{1 + \sqrt{R}}{1 - \sqrt{R}} + \sqrt{\frac{4R}{(1 - R)^2}} - K^2.$$
 (13)

Figure 7 illustrates the correlation between the refractive index and the energy of a photon. It is observed that the refractive index curve exhibits a drop as the energy of the photon surpasses the energy gap, particularly at higher energy levels. The findings indicate that the refractive

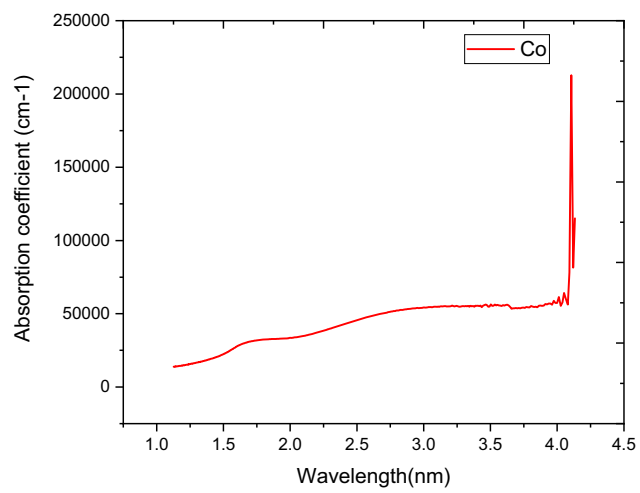


Figure 6: Absorption coefficient relation photon energy for CoNPs.

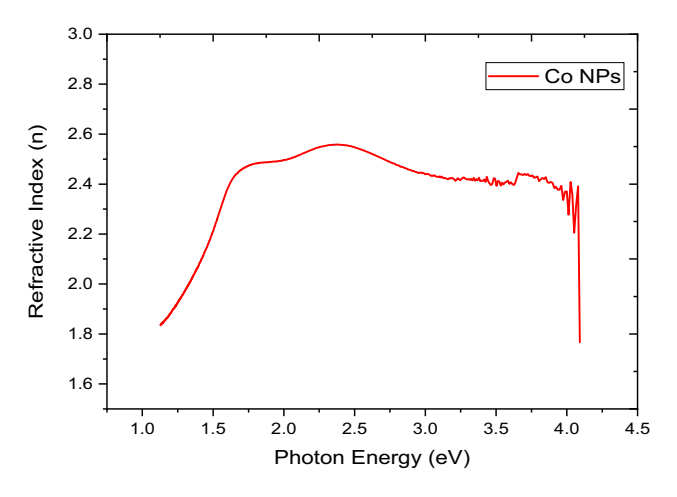


Figure 7: Refractive index relation photon energy for CoNPs.

index at the membrane reaches its peak value at 2.5881. Subsequently, the refractive index coefficient increases as the energy of the photon increases until it reaches its maximum value at 2.3 eV. Afterward, it decreases and reaches 1.766 when the photon energy is 4.2 eV. This decrease can be attributed to an increase in compaction, resulting in a decrease in the speed of light propagation within the material. It is important to note that the refractive index is influenced by the material type and its crystal structure.

The energy of the incident photons as well as the properties of the material, which include energy gaps and various kinds of electronic transmission that take place between frequency bands, determines the absorption coefficient.

The optical energy gap's magnitude is one of the most fundamental optical parameters that is impacted by matter structure. Equation Tauc (14) with r = 1/2 [10] restricts the CoNPs Co films energy gap for permitted direct electronic transitions:

$$\alpha h v = \beta (h v - E_g)^r, \tag{14}$$

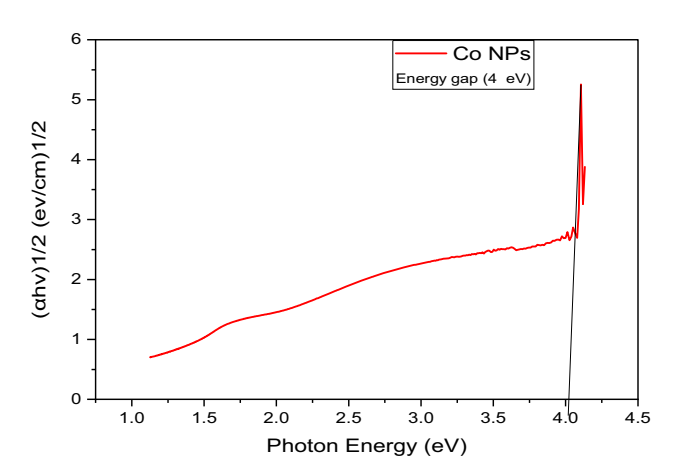


Figure 8: Variation for the $(\alpha hv)^{1/2}$ with the incident photon energy for CoNPs.

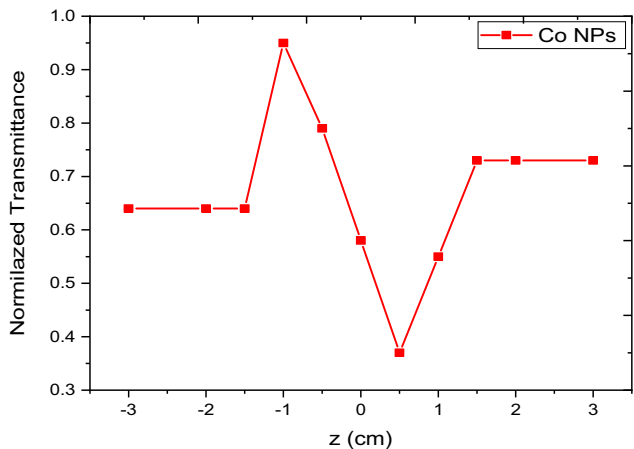


Figure 9: The normalized transmittance curve of CoNPs at a 650 nm wavelength with a power of 50 mW as a function of position.

where α is the absorption coefficient, β is the constant dependent on effective mass and medium density, h is the Plank constant, and v is the incident photon frequency. Additionally, the constant r assumes different values (3, 2, 2/3, 1/2) depending on the specific type of electronic transitions responsible for the optical absorption [10].

In order to cut the photon energy axis at the position $(h\nu) = 0$, the straight section is drawn to connect $(\alpha h\nu)^{\frac{1}{2}}$ and photon energy $(h\nu)$. According to Figure 8, the CoNP films' energy gap to direct transition is 4 eV.

3.3.2 Nonlinear optical properties

Figures 9 and 10 illustrate the empirical results acquired by employing the Z-scan technique on CoNPs positioned on a

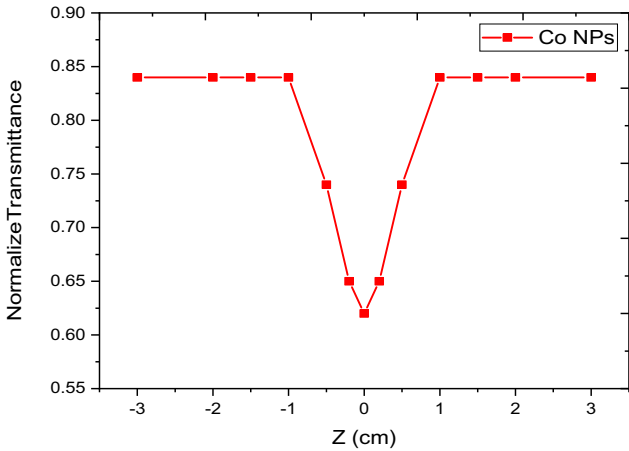


Figure 10: The normalized transmittance curve for CoNPs at 650 nm with a power of 50 mW as a function of position.

Table 2: Result of nonlinear optical properties for CoNP films by Z-scan technique

λ(nm)	Power of laser (mW)	Ư (Rad)	ΔT_{P-V}	$n \times 10^{-15} \text{ (cm}^2/\text{mW)}$	$\Delta n \times 10^{-13}$	T _{max}	$\beta \times 10^{-8}$ (cm/mW)	χ ⁽³⁾ ×10 ⁻⁸
650	50	1.428571	0.58	2.64	3.37	20.6	6.65	2.87

glass substrate. The studies were carried out using both closed and open apertures, utilizing continuous wave diodes operating at a power output of 50 mW at a wavelength of 650 nm. The nonlinear optical coefficients of CoNP films were compiled. The determination of the third-order nonlinear optical susceptibility, denoted as $|\chi^{(3)}|$, can be achieved by employing equation (11). Similarly, the calculation of the nonlinear absorption coefficient, represented as β , can be obtained using equation (8). The evaluation of the nonlinear refraction index, denoted as n_2 , can be accomplished by applying equation (6). Additionally, the assessment of the change in refraction index, indicated as Δn , can be obtained by utilizing equation (7). These equations provide a means to quantify these various quantities of interest.

The transmittance curve of CoNP, which is influenced by various positions in the close aperture Z-scan, is depicted in Figure 9. Similarly, Figure 10 illustrates the transmission curve of CoNPs, which exhibits dependence on various locations within the open aperture Z-scan. The determination of the nonlinear refraction index involves calculating the ratio of the transmission magnitudes of a laser beam with a closed aperture to the transmission magnitudes without an aperture. This process is demonstrated in Figures 8 and 9. The nonlinear refraction index n_2 was determined to be 2.64 \times 10⁻¹⁵ cm²/mW at a wavelength of 650 nm, by the analysis of Zscan operations performed on CoNP films. Furthermore, the value of the nonlinear absorption coefficient β was determined to be 6.65×10^{-8} cm/mW at the wavelength of 650 nm, employing a power of 50 mW. As evidenced by the data presented in Table 2, the value of the third-order nonlinear optical susceptibility $\chi^{(3)}$ is determined to be 2.87 × 10⁻⁸ at a wavelength of 650 nm and a power of 50 mW.

The Z-scan technique was employed to investigate the optical properties of films containing CoNPs. It was found that these films exhibit a self-defocusing effect and display two-photon absorption, as observed in both closed and open apertures. Additionally, it has been observed that films containing CoNPs demonstrate a substantial level of the third-order nonlinear optical susceptibility.

4 Conclusion

The CoNPs were synthesized using a pulsed Nd-YAG laser operating at a wavelength of 1,064 nm and an energy of 800 mJ. The synthesis process involved dispersing the NPs in water and subsequently depositing them onto glass substrates. From the results of the structural and morphological attributes of CoNP films, it is evident that CoNPs exhibit different spherical configurations with diameters spanning from a few nanometers to 24 nm. The surfaces of these CoNP films are noticed to indicate that they exhibit a certain degree of homogeneity and uniform vertical heights. Additionally, the results demonstrate an increase in granular size growth and the emptying of cavities on the material's surface. The absorption spectra exhibited a prominent peak at a wavelength of 300 nm, accompanied by further peaks spanning the range of 400-700 nm. The optical constants and energy gap were determined through the analysis of absorbance and transmittance measurements. The experimental findings pertaining to the nonlinear optical characteristics of CoNP films revealed the presence of two-photon absorption and nonlinear refraction index self-defocusing. Consequently, it can be inferred that CoNPs possess good nonlinear properties and can be used in nonlinear optical photonic devices, optical power limiters, and a wide range of nonlinear applications.

Author contributions: MLD contributed to the experimental work, analyzing the scientific results, and drawing the graphics that appeared in the manuscript. AG contributed by writing the introduction to the research and providing technical supervision for writing the manuscript. SAH contributed by writing the summary and conclusion.

Conflict on interest: Authors state no conflict of interest.

Data availability statement: The most datasets generated and/or analysed in this study are comprised in this submitted manuscript. The other datasets are available on reasonable request from the corresponding author with the attached information.

References

Dubchak S, Ogar A, Mietelski JW, Turnau K. Influence of silver and titanium nanoparticles on arbuscular mycorrhiza colonization and accumulation of radiocaesium in Helianthus annuus. Span J Agric Res. 2010;(1):103-8.

- [2] Khusnuriyalova AF, Caporali M, Hey-Hawkins E, Sinyashin OG, Yakhvarov DG. Preparation of cobalt nanoparticles. Eur J Inorg Chem. 2021 Aug;2021(30):3023–47.
- [3] Drmosh QA, Gondal MA, Yamani ZH, Saleh TA. Spectroscopic characterization approach to study surfactants effect on ZnO2 nanoparticles synthesis by laser ablation process. Appl Surf Sci. 2010 May;256(14):4661–6.
- [4] Imran HJ, Hubeatir KA, Aadim KA, Abd DS. Preparation methods and classification study of nanomaterial: A review. J Phys: Conf Ser. 2021 Mar;1818(1):012127. IOP Publishing.
- [5] Kim KK, Kim D, Kim SK, Park SM, Song JK. Formation of ZnO nanoparticles by laser ablation in neat water. Chem Phys Lett. 2011 Iul:511(1–3):116–20.
- [6] Acacia N, Barreca F, Barletta E, Spadaro D, Currò G, Neri F. Laser ablation synthesis of indium oxide nanoparticles in water. Appl Surf Sci. 2010 Sep;256(22):6918–22.
- [7] Phuoc TX, Soong Y, Chyu MK. Synthesis of Ag-deionized water nanofluids using multi-beam laser ablation in liquids. Opt Lasers Eng. 2007 Dec;45(12):1099–106.
- [8] Pramodini S, Sudhakar YN, SelvaKumar M, Poornesh P. Studies on third-order optical nonlinearity and power limiting of conducting polymers using the z-scan technique for nonlinear optical applications. Laser Phys. 2014 Mar;24(4):045408.
- [9] Neethling PH. Determining non-linear optical properties using the Z-scan technique. Doctoral dissertation. Stellenbosch: University of Stellenbosch.
- [10] Chapple PB, Staromlynska J, Hermann JA, Mckay TJ, McDuff RG. Single-beam Z-scan: Measurement techniques and analysis. J Nonlinear Opt Phys Mater. 1997 Sep;6(3):251–93.
- [11] Fontalvo M, García A, Valbuena S, Racedo F. Measurement of nonlinear refractive index of organic materials by z-scan. J Phys: Conf Ser. 2016 Feb;687(1):012100. IOP Publishing.

- [12] Shahriari E, Yunus WM. Effect of particle size on nonlinear refraction and absorption of Ag nanoparticles. Dig J Nanomater Biostruct. 2010 Oct;5(4):939–46.
- [13] Kumaresan S, Ahamed MB. Single beam Z-scan measurement of the third order optical nonlinearities of styryl7 dye. Optik. 2014 Oct;125(20):6152–4.
- [14] Kumari V, Kumar V, Malik BP, Mehra RM, Mohan D. Nonlinear optical properties of erbium doped zinc oxide (EZO) thin films. Opt Commun. 2012 Apr;285(8):2182–8.
- [15] Sheik-Bahae M, Said AA, Wei TH, Hagan DJ, Van Stryland EW. Sensitive measurement of optical nonlinearities using a single beam. IEEE J Quantum Electron. 1990 Apr;26(4):760–9.
- [16] Rahman MA, Alghoraibi I. Theoretical investigation of second harmonic efficiency effect on third harmonic conversion efficiency in BBO crystals. Optik. 2019 Oct;194:163031.
- [17] Rao KS, Ganeev RA, Zhang K, Fu Y, Boltaev GS, Krishnendu PS, et al. Laser ablation–induced synthesis and nonlinear optical characterization of titanium and cobalt nanoparticles. J Nanopart Res. 2018 Oct;20:1–5.
- [18] Li J, Liu CY, Xie Z. Synthesis and surface plasmon resonance properties of carbon-coated Cu and Co nanoparticles. Mater Res Bull. 2011 May;46(5):743–7.
- [19] Simon G, Meziane L, Courty A, Colomban P, Lisiecki I. Low wavenumber Raman scattering of cobalt nanoparticles self-organized in 3D superlattices far from surface plasmon resonance. J Raman Spectrosc. 2016 Feb;47(2):248–51.
- [20] Duque JS, Blandón JS, Riascos H. Localized Plasmon resonance in metal nanoparticles using Mie theory. J Phys: Conf Ser. 2017 Jun;850(1):012017. IOP Publishing.
- [21] Kaminskienė Ž, Prosyčevas I, Stonkutė J, Guobienė A. Evaluation of optical properties of Ag, Cu, and Co nanoparticles synthesized in organic medium. Acta Phys Polonica A. 2013 Jan;123(1):111–4.